



Sigmoid Type Neuromorphic Activation Function Based on Saturable Absorption Behavior of Graphene/PMMA Composite for Intensity Modulation of Surface Plasmon Polariton Signals

Hamed Tari¹ · Alessandro Bile¹ · Francesca Moratti¹ · Eugenio Fazio¹

Received: 28 January 2021 / Accepted: 4 October 2021 / Published online: 21 January 2022
© The Author(s) 2022

Abstract

For an optical technology to be feasible as a substitution of electronics one for neuromorphic applications, it is required the waveguides in which are capable of confining and directing light signals in much smaller dimensions than the operating wavelength of the light, i.e., subwavelength optical components must be realized. Hybrid nature of surface plasmon polariton addresses the problem with the diffraction limit of regular photonic components. Here, the authors present a two-dimensional numerical simulation of a passive photonic element based on a saturable absorber material as a hardware base analogy to the biological activation function existed at the cell body of neurons. They demonstrate that at telecom wavelengths, a highly confined SPP mode can be modulated in a nonlinear fashion by considering the carrier dynamics of graphene/PMMA polymeric composite as a two-level system. The hardware base sigmoid type nonlinear activation function derived from this study further characterized; and the parameters which appeared to be effective on the performance of the structure, such as saturation intensity, modulation depth, and thickness of the synaptic part as a Fabry–Pérot structure, have been studied.

Keywords Neuromorphic activation function · Surface plasmon polariton · Photonic synapse · Saturable absorber

Introduction

So far, artificial neural networks (ANNs) have been mostly implemented in software approaches. It is beneficial since the designer does not need to be aware of the mechanism in which how the neural network elements work but can focus on the application of the neural network. Nevertheless, the drawback in real-time applications of software-based ANNs is slower performance compared with hardware-based ANNs. Hardware execution of ANNs is relatively rare and, here [1, 2], it is possible to find some representative

examples of recent researches. Till now, the implementation of these functions was performed by software approach, and most computers still use the Von Neumann architecture which suffers the low performances due to the time latency of the memory and processor. Actually, a hardware implementation is feasible due to the ever-increasing possibilities of electronic and photonic integrated circuits in which their coexistence solves most of the problems related to the low bandwidth and energy efficiency of electronic circuits and bulky large size of the photonic integrated circuits. Recently, 1D nanowires or nanofibers, with their diameters ranging from tens to hundreds of nanometers and lengths up to tens of millimeters, have attracted major interest in photonic applications [3]. Generally, photonic nanowires, such as semiconductor nanowires [4], nonlinear optical crystals waveguide [5], glass nanofibers [6], or silicon-on-insulator waveguides [7], exhibit low optical waveguiding losses, but their optical confinement is limited by the diffraction limit that is on the order of λ/n (with $n < 5$). In contrast, by coupling light to the collective oscillations of electron on the noble metal interface and a dielectric layer, the electromagnetic field of the photons can be trapped on the surface due to its interaction with the free conduction electrons of the

✉ Hamed Tari
Hamed.tari@uniroma1.it

Alessandro Bile
Alessandro.bile@uniroma1.it

Francesca Moratti
Francesca.moratti3@gmail.com

Eugenio Fazio
Eugenio.fazio@uniroma1.it

¹ Department of Basic and Applied Sciences for Engineering, Sapienza University of Roma, 00161 Roma, Italy

metal. The hybrid nature of SPP makes it possible to simultaneously carry optical and electrical signals in the same circuitry and interact properly with the electronic and photonic components. Moreover, the high localization and surface confinement of surface plasmon polariton (SPP), greatly enhance the intensity at the 2-dimensional (2D). This hybrid characteristic of the SPP collects the advantages of photonic (such as higher bandwidth and higher speed) and electronic technology (the higher interaction and lower size and wavelength) and enables the design of the computationally fast and highly dense neural network, and provides vast variety of application such as magneto-plasmonic switch based on SPP [8] and metamaterials for sensing applications [9].

Unrestricted by the diffraction limit, plasmonics structures can enable stronger modal confinement to enhance optical processes and miniaturize photonic circuits. Though, the electromagnetic waves at telecom frequency can be tightly confined along with the interface of a metal and a dielectric layer, and guide the light beyond the diffraction limit in a metal nano strip [10]. However, despite that the wider metal stripes can effectively guide the SPP, nevertheless, when the width of the stripe becomes smaller, the losses significantly increase due to scattering on the stripe edges, preventing scaling down such waveguides. In order to overcome this problem, dielectric waveguides for SPPs on a metal surface have been recently proposed [11]. The dielectric results in a higher refractive index for an SPP wave on a metal–dielectric interface compared to the metal–air interface, giving rise to SPP modes bound by the dielectric stripe similar to the guided light modes in conventional optical fibers or planar dielectric waveguides. Thus, stronger confinement and reduction of edge-scattering losses in dielectric-loaded SPP waveguides (DLSPWs) can be achieved compared to bare metallic stripe waveguides of the same width. Moreover, a dielectric coating can be functionalized to provide thermo, electro, or all-optical functionalities and can be used for the development of active and passive modulation of plasmonics components.

Compared to the active SPP modulation, the passive modulation of SPP, which is based on the nonlinear interaction of the material to the light, has advantages in compactness,

lower complexity of integration, low cost, etc. The Kerr effect and saturable absorption are the main phenomena used in passive optical modulators, both of which represent third-order optical nonlinearities, where the former is determined by the real part of the optical susceptibility and the latter is related to the imaginary part. Compared with the Kerr effect, saturable absorption is a modulation of the absorption and has advantages in some aspects, such as tunable and large modulation depth. However, along the generated losses during saturable absorption process which is determined by the sensitivity of the absorption to light intensity, the indirect 1.12 eV band-gap of silicon limits its application in passive modulators and detectors especially at telecommunications wavelengths, e.g., 1.3 (0.95 eV) and 1.5 μm (0.8 eV) [12–14]. Zhang et al. [15] have recently reported that graphene can provide outstanding saturable absorption, overcoming these inherent drawbacks of semiconductor saturable absorber materials. Because of its unique energy band properties with the Pauli blocking principle, graphene possesses significant advantages, including ultra-low saturation intensity, larger saturable-absorption modulation depth, higher damage threshold, ultrafast recovery time, and a broad wavelength-independent saturable absorption range (300–2500 nm) [16].

Here, what the study intends to accomplish is to numerically simulate a photonic neuron based on SPP for neuromorphic application purposes. The neuron consists of a saturable absorber that is responsible for the nonlinear transmission of the SPP. The saturable absorber defines a threshold value for the transmission of incoming SPP field and as a result, its intensity undergoes a passive and nonlinear modulation. It has been demonstrated that at telecom wavelengths, a highly confined SPP mode can be modulated in a nonlinear fashion by considering the carrier dynamics of graphene/PMMA polymeric composite as a two-level system. The saturable absorber behavior of the graphene/PMMA results to a sigmoid type non-linear activation function, and the parameters which appeared to be effective on the performance of the neuron, such as saturation intensity, modulation depth, and thickness of the saturable absorber have been optimized accordingly.

Fig. 1 (A) Schematic representation of the simulated structure. (B) Excitation of the structure with a periodic port with intensity before saturation intensity of the saturable absorber and complete suppression of the SPP field

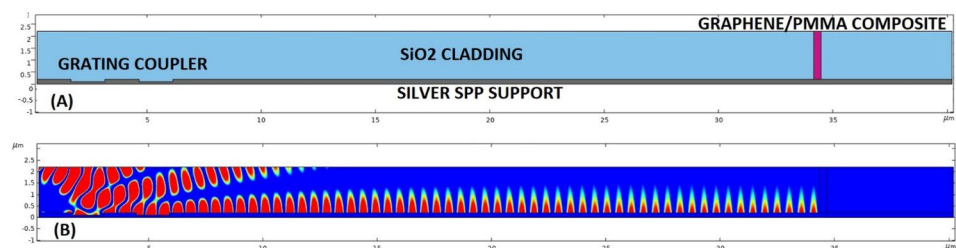


Table 1 Different material optical properties and SPP propagation parameters: SPP wavelength, propagation length for decay of intensity of SPP by 1/e, penetration depth of SPP in metal layer, penetra-

tion depth in dielectric layer, normalized intensity for SPP received at the end of structure, and finally the grating wavelength (groove width) respectively

Materials	<i>n</i>	λ_{SPP} (μm)	L_{SPP} (μm)	δ_m (nm)	δ_d (μm)	I_{SPP} (W/cm ²)	λ_g (μm)
SiO ₂	1.444	1.0734	406	21.53	1.334	1.9144	1.420
Photoresist	1.575	0.9834	311	21.49	1.119	1.2912	1343
AlN/Al ₂ O ₃	1.765	0.8781	220	21.44	0.889	0.9294	1.246
Al _x Ga _{1-x} As	3.243	0.4776	32	20.8	0.255	0.0589	0.795
In _x Ga _{1-x} As _{1-y} P _y	3.248	0.4767	32	20.8	0.254	0.0745	0.794
Si	3.476	0.4459	26	20.6	0.221	1.1509	0.751
In _x Ga _{1-x} As	3.536	0.4389	5	20.6	0.213	2.01E-10	0.740

Simulation Method

Since the plasmon effect is essentially a near-field phenomenon, only near field in this simulation is calculated. We have started with 2D simulations in order to be able to use extra fine mesh for higher preciseness. All domain boundaries except the bottom of the Ag strip are surrounded by perfectly matched layer (PML) to absorb outgoing waves. The skin depth of Ag at visible wavelength is about 20 nm, so the transmission through 100-nm Ag film is negligible, and no PML is needed at the bottom boundary. PML at the top boundary assumes infinite half space for SiO₂ interface. Note that special care needs to be taken for PML set up at the metal/dielectric interface region for appropriate absorption of the SPP waves. It has to be noted, at higher values of the input power, still a small portion of the light reflects back inside the propagation area; and in order to prevent their interference with the SPP, we have considered the outermost boundary of the PML as second-order scattering boundary condition which ensures nearly zero back reflection of the light inside the propagation area.

A periodic port has been utilized to illuminate the structure at the grating region to couple the light to SPP. Figure 1 represents the schematic view of the simulated structure with 1-mW input power. The SPP propagates along the metal/dielectric interface and shows a great surface confinement. Since the intensity of the received SPP is lower than the saturation intensity of the saturable absorber, so the SPP field is completely suppressed, and no SPP is able to be transmitted to the post synaptic region.

Effect of Different Dielectric Materials on SPP Propagation

The important parameter, which has been analyzed here, is the material sweep for studying the effect of different dielectric materials to the SPP propagation. The selected materials in this simulation have been taken from the most popular

materials in the semiconductor industry which all of them are CMOS compatible and fabrication of them is commercially available. Table 1 summarizes the calculated parameters for different materials. According to these data, it is possible to vary the SPP wavelength simply by changing the dielectric material and cover a broad range of wavelengths. Taking into account the imaginary part of the propagation constant, it is possible to calculate the length $L_{SPP} = 1/2k''_{SPP}$ in which the SPP field intensity can propagate along the interface with a decay factor of 1/e by considering the k''_{SPP} parallel to the interface as follow

$$k''_{SPP,x} \approx \frac{\omega}{c} \sqrt{\frac{\epsilon'_1 \epsilon_2}{\epsilon'_1 \epsilon_2}} \frac{\epsilon''_1 \epsilon_2}{2\epsilon'_1(\epsilon'_1 + \epsilon_2)} \tag{1}$$

$$k_{1,z} = \frac{\omega}{c} \sqrt{\frac{(\epsilon'_1)^2}{\epsilon'_1 + \epsilon_2}} \left[1 + i \frac{\epsilon''_1}{2\epsilon'_1} \right] \tag{2}$$

$$k_{2,z} = \frac{\omega}{c} \sqrt{\frac{(\epsilon'_1)^2}{\epsilon'_1 + \epsilon_2}} \left[1 - i \frac{\epsilon''_1}{2(\epsilon'_1 + \epsilon_2)} \right] \tag{3}$$

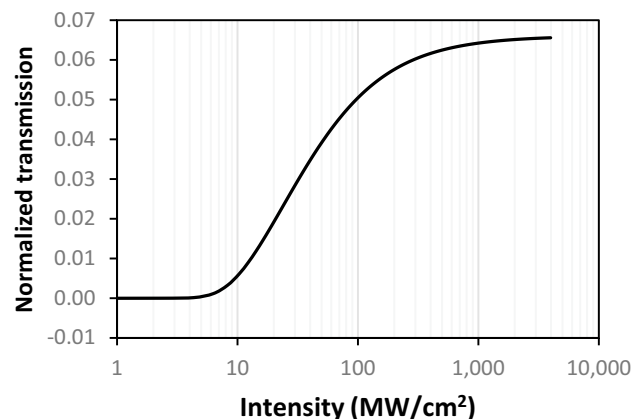


Fig. 2 Nonlinear transmission curve as a function of the input port intensity for graphene polymeric composite at 1550-nm wavelength

where the ε_1 and ε_2 are the permittivities of the metal and dielectric layer respectively. From the collected data for different dielectric materials, it is clear that, to have a long propagation length along the interface and penetration depth of SPP normal to the interface, it is required to implement a dielectric material with a lower refractive index. The highest propagation length belongs to the SiO₂ which its lower refractive index allows the SPP to propagate about 400 μm along with the interface. The lowest value for SPP propagation length is for InGaAs, which no matter how much the angle of incidence is, the propagation length barely reaches to 5 μm . To calculate how much SPP

is able to penetrate inside the metallic layer (δ_m) and the dielectric layer (δ_d), we have implemented Eqs. (2) and (3) respectively. The electric field penetration depth of SPP for metal and dielectric layer is $1/k_{1,z}$ and $1/k_{2,z}$ respectively. The penetration depth for the metallic layer is almost the same for all of the materials but for the dielectric materials changes in a broad range. As a result, for a more confined SPP field inside the dielectric layer, one can use a dielectric material with a higher refractive index. From the obtained results, the highest value of field penetration inside the dielectric layer belongs to the SiO₂, and the lowest value belongs to Si and InGaAs.

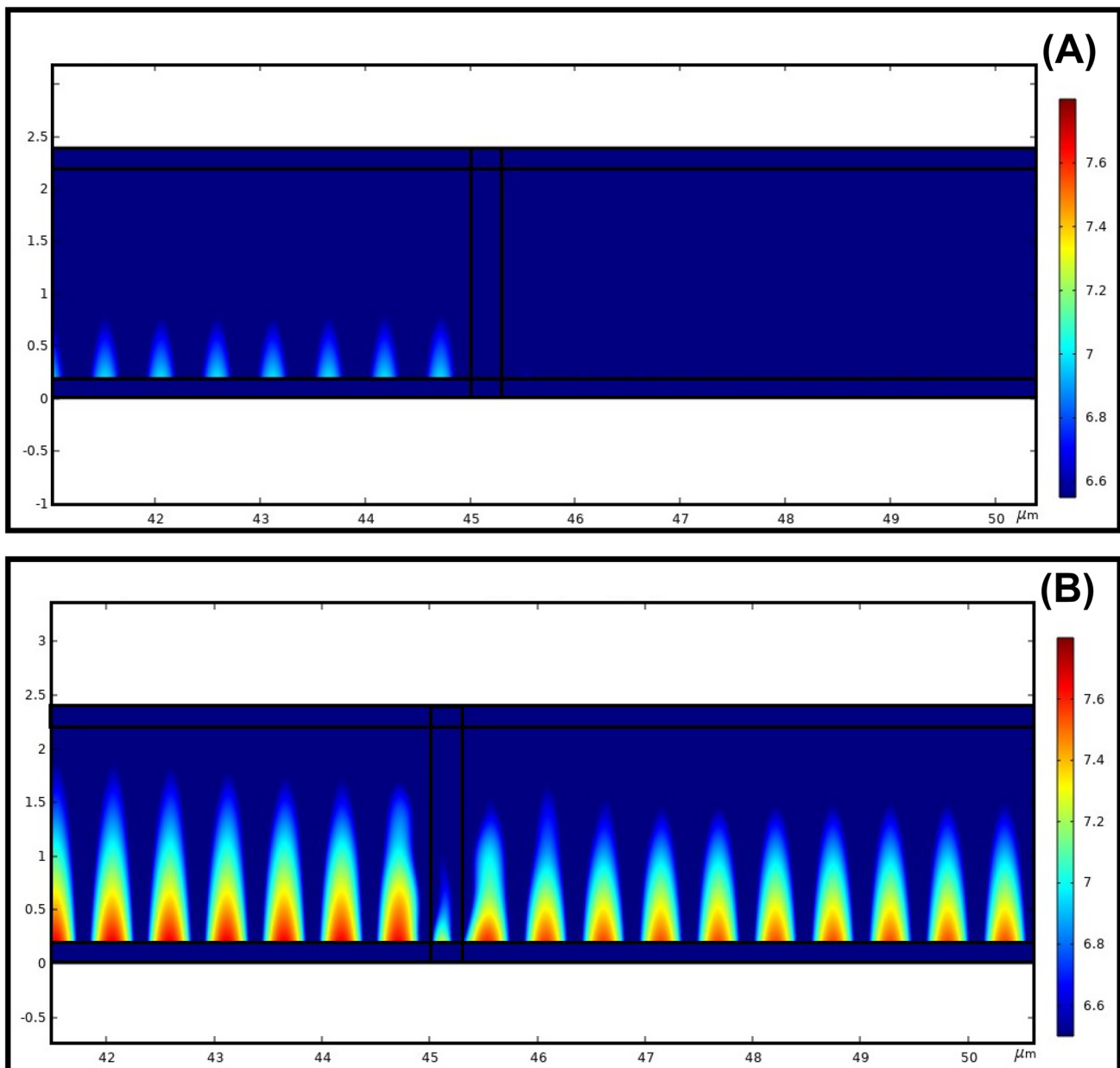


Fig. 3 SPP intensity profile (A) before reaching to the saturation intensity and (B) after reaching to the saturation intensity of graphene polymeric composite

Saturable Absorber Behavior of Graphene Polymeric Composite

The optical properties of the composite material (graphene/PMMA) such as saturable and nonsaturable absorption coefficients, photo-induced electron–hole density, and carrier recombination time have been obtained from the recently published papers [17, 18] which will be elaborated here. In this section, in order to consider the carrier dynamics of graphene/PMMA inside the Maxwell’s equation, we have implemented the macroscopic polarization vector as follows:

$$D = \epsilon_0 \epsilon_h E + \sum_m P_m \tag{4}$$

in which the ϵ_h is the permittivity of the host material (here we have used PMMA as the host for graphene nanoflakes) and P_m is the polarization induced by the m^{th} oscillator. Taking into consideration, a source term-dependent to the difference of the population density in ground state and excited level, it is possible to define the macroscopic polarization by an auxiliary differential equation (ADE) as follows:

$$\frac{d^2 P_{10}}{dt^2} + \gamma_{10} \frac{dP_{10}}{dt} + \omega_0^2 P_{10} = \kappa_{10} (N_0 - N_1) E_y \tag{5}$$

where P_{10} is the average macroscopic polarization vector, which is a function of time and space, γ_{10} is the damping coefficient of this oscillator, and the ω_0 is the transition frequency. The coupling factor κ_{10} takes the form of $\kappa_{10} = 6\pi N_d \epsilon_0 c^3 / (\tau_{10} \omega_0^2 \sqrt{\epsilon_h})$ where $N_d = C_{\text{graph}} \cdot N_A$, in which represents the concentration of the graphene nanoflakes (here we have used 0.01 M for the concentration) distributed in the matrix of the PMMA, and N_A is the Avogadro constant, and τ_{10} is the relaxation time of the transition from

excited state to the ground state. By considering the graphene/PMMA as a two-level system, the transition between this two levels can be described with an ADE as follows:

$$\frac{dN_1}{dt} = -\frac{N_1}{\tau} + \frac{1}{\hbar \omega_0} E_y \cdot \frac{dP}{dt} \tag{6}$$

here the population density of the excited state and ground state is expressed as N_0 and N_1 . By adding these equations as two ADEs, we can relate the Maxwell’s equation to the carrier dynamic of the polymeric composite in saturable absorber part.

As can be seen from the Fig. 2, there is an S shape trend in the transmission of SPP which represents the saturation behavior of the absorption coefficients. From this experiment, we have found that the saturation intensity is 53.5-MW/cm² for a layer of SA with 200-nm thickness and is strongly dependent to the concentration of the graphene nanoflakes and also the thickness of the composite material. The modulation depth for this structure is about 6%. This nonlinear transmission curve shows a perfect compatibility to the activation curve of sigmoid type which is an essential element in the neuromorphic applications. Figure 3 indicates the two state of the system, (A) before reaching the saturation intensity which occurs in low input power and (B) after reaching the saturation intensity. Since the intensity of SPP is lower in the (A), it is completely suppressed by the SA and no field is transmitted, but when the intensity of the SPP passes through the saturation threshold, part of the SPP intensity transmits to the other side of the structure in post synaptic region. In order to further analyze this nonlinear activation function, it has been set up a simulation to further investigate the effect of the thickness of the saturable absorber layer on the saturation intensity and the modulation depth.

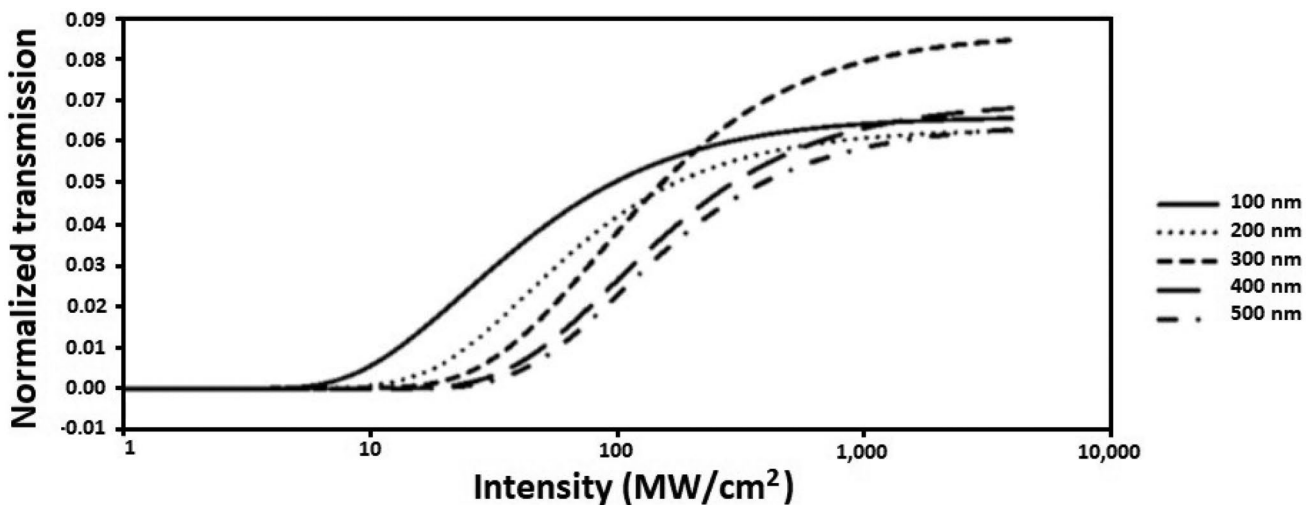


Fig. 4 Effect of different thickness of saturable absorber layer on the saturation behavior of the graphene/PMMA composite

Effect of the Thickness and Concentration of Graphene Nanoflakes on Saturation Intensity

In order to see what is the effect of saturable absorber thickness on the modulation depth and saturation intensity (defined as the SPP intensity required to reduce the absorption to half of its unbleached value), we have studied the model in the previous section with different SA thickness, ranging from 100 to 500 nm. The lowest saturation intensity as depicted in occurs for 100-nm thickness which is about 34.1 MW/cm^2 . By increasing the thickness of the SA layer, since the absorption length is increasing, as a result, we will

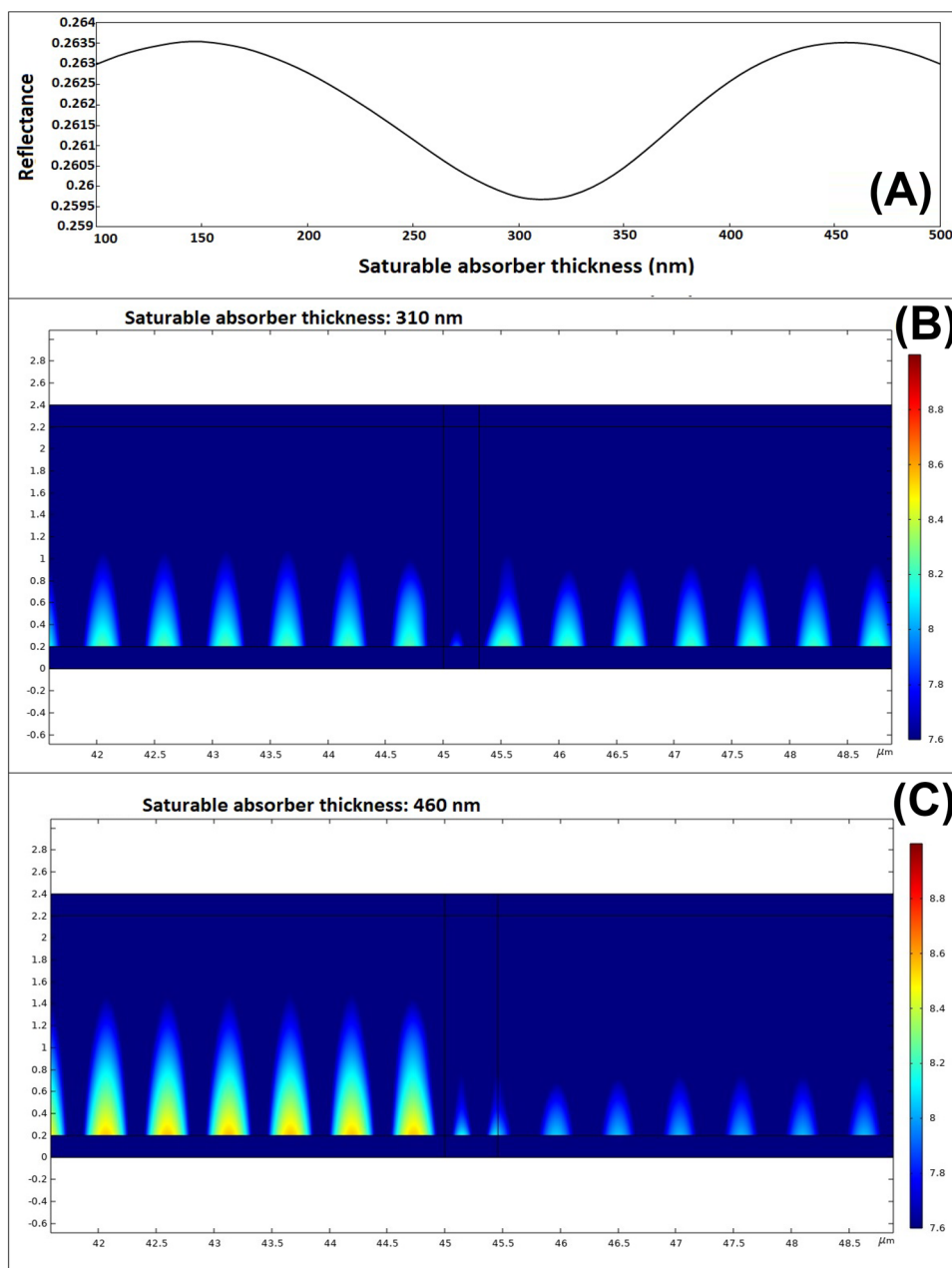
have saturation at higher intensities and the curves shift to the higher values. From the Fig. 4, it is clear that the modulation depth for all of the thickness values is nearly the same and lies between 6 and 7%, but for the 300 nm, this value is about 8.5%.

Since in this simulation we have a normal incidence of SPP field to the SA layer, so we have two conditions for the interference of the back-reflected light as follows:

$$2n_{SA}d_{SA} = (m - \frac{1}{2})\lambda_0 \text{ for constructive interference of reflected light} \quad (7)$$

$$2n_{SA}d_{SA} = m\lambda_0 \text{ for destructive interference of reflected light} \quad (8)$$

Fig. 5 (A) Reflectance of SPP for different values of saturable absorber thickness from 100 to 500 nm. (B) Graphical representation of the SPP reflectance magnitude at minimum values of 310 nm and (C) maximum at 460 nm



So in order to prevent the back reflection of the SPP and increase the transmission to the other side of the structure, it is required to have a thickness of the SA equal to $d_{SA} = \frac{m\lambda_0}{2n_{SA}} = \frac{1550nm}{2 \times 2.4793} = 312nm$, for $m=1$. This is the reason why we observed the higher modulation depth for the SA with 300-nm thickness. Figure 5A indicates further explanation for this observation which represents the reflectance of SPP by sweeping the SA thickness from 100 to 500 nm. The results show a periodic trend with a minimum value of the reflectance around 310 nm which is compatible with derived value of 312 nm and a maximum value of reflectance at 460 nm. This result is also represented visually in Fig. 5B, C in which the transmission of SPP is reduced because of the high reflection at 460 nm of thickness. This is the reason why by increasing the thickness of the SA layer, we observe a reduction in the modulation depth of SA. The similar trend was also observed for the effect of the concentration of the graphene nanoflakes (related data is not presented) in which by increasing the concentration, the saturation intensity increased as well. For avoiding extra losses related to the higher concentration of the SA and also preventing the agglomeration, it is convenient to use low concentration of the nanoflakes in the range of 0.005 to 0.01 which provides the saturation intensity ranging from 34.6 to 53.5 MW/cm² for a composite of 200-nm thickness.

Conclusion

Taking into account the results of this study, it is possible to demonstrate a fully functioning all-optical nonlinear activation function, based on the saturable absorber property of graphene/PMMA. The synaptic behavior of this saturable absorber material provides a passive saturable optical response for the SPP signal. All of the optical properties of the graphene have been adopted from the recent experimental works, and the results of this simulation are closely consonant with those results. The demonstrated SA scheme can be used to construct various neuromorphic architectures with intrinsic and passive optical computation. The maximum value for the modulation depth is possible for the thickness of 310 nm and is equal to 8.5% which compared to the other values of thickness is considerable. This behavior is mainly because of the destructive interference of the back-reflected SPP field which is reflected from the second interference and reduces the reflection coefficient of intensity. As a result, the transmitted SPP intensity is higher in 310-nm thickness and this trend repeats periodically.

Author Contribution All authors contributed to the study conception and design. COMSOL numerical analysis and data collection were performed by Dr. Hamed Tari. COMSOL environment was set up by Dr. Alessandro Bile. Professor Eugenio Fazio provided the workstations

and technical assistance during the COMSOL calculations. The first draft of the manuscript was written by Francesca Moratti.

Funding This study received financial support from the Department of Basic and Applied Science for Engineering of Sapienza University of Rome (Avvio alla Ricerca, Sapienza University of Rome AR120172B7152382).

Data Availability The data that support the findings of this study are available from the corresponding author upon reasonable request.

Declarations

Ethics Approval There is no ethical approval required. “Not applicable.”

Consent to Participate Informed consent was obtained from all individual participants included in the study. Not applicable.

Consent for Publication Authors are responsible for the correctness of the statements provided in the manuscript.

Conflict of Interest The authors declare no competing interests.

Open Access This article is licensed under a Creative Commons Attribution 4.0 International License, which permits use, sharing, adaptation, distribution and reproduction in any medium or format, as long as you give appropriate credit to the original author(s) and the source, provide a link to the Creative Commons licence, and indicate if changes were made. The images or other third party material in this article are included in the article's Creative Commons licence, unless indicated otherwise in a credit line to the material. If material is not included in the article's Creative Commons licence and your intended use is not permitted by statutory regulation or exceeds the permitted use, you will need to obtain permission directly from the copyright holder. To view a copy of this licence, visit <http://creativecommons.org/licenses/by/4.0/>.

References

1. Tommiska M (2003) Efficient digital implementation of the sigmoid function for reprogrammable logic. *IEE Proc Comput Digit Tech* 150(6):403–411
2. Bile A, Moratti F, Tari H, Fazio E (2021) Supervised and unsupervised learning using a fully-plastic all-optical unit of artificial intelligence based on solitonic waveguides. *Neural Comput Applic* 1–9
3. Rosenbluth D, Kravtsov K, Fok MP, Prucnal PR (2009) A high performance photonic pulse processing device. *Opt Express* 17(25):22767–22772
4. Lu W, Lieber CM (2006) Semiconductor nanowires. *J Phys D Appl Phys* 39(21):R387
5. Fazio E, Chauvet M, Vlad V, Petris A, Pettazzi F, Coda V, Alonzo M (2014) 3-D Integrated optical microcircuits in lithium niobate written by spatial solitons. In: *Ferroelectric Crystals for Photonic Applications*. Springer, pp 99–132
6. Tong L, Sumetsky M (2009) Subwavelength and nanometer diameter optical fibers Zhejiang. Zhejiang University Press
7. Dumon P, Bogaerts W, Wiaux V, Wouters J, Beckx S, Van Campenhout J, Taillaert D, Luyssaert B, Bienstman P, Van Thourhout D (2004) Low-loss SOI photonic wires and ring resonators fabricated with deep UV lithography. *IEEE Photonics Technol Lett* 16(5):1328–1330

8. Bile A, Pepino R, Fazio E (2021) Study of magnetic switch for surface plasmon-polariton circuits. *AIP Adv* 11(4):045222
9. Tang W, Wang L, Chen X, Liu C, Yu A, Lu W (2016) Dynamic metamaterial based on the graphene split ring high-Q Fano-resonator for sensing applications. *Nanoscale* 8(33):15196–15204
10. Maier SA (2007) *Plasmonics: fundamentals and applications*. Springer-Verlag, Berlin, p 89
11. Reinhardt C, Passinger S, Chichkov BN, Marquart C, Radko IP, Bozhevolnyi SI (2006) Laser-fabricated dielectric optical components for surface plasmon polaritons. *Opt Lett* 31(9):1307–1309
12. Avrutsky I, Soref R (2011) Phase-matched sum frequency generation in strained silicon waveguides using their second-order nonlinear optical susceptibility. *Opt Express* 19(22):21707–21716
13. Wang L, Chen X, Lu W (2015) Intrinsic photo-conductance triggered by the plasmonic effect in graphene for terahertz detection. *Nanotechnol* 27(3):035205
14. Liu C, Wang L, Chen X, Politano A, Wei D, Chen G, Tang W, Lu W, Tredicucci A (2018) Room-temperature high-gain long-wavelength photodetector via optical–electrical controlling of hot carriers in graphene. *Adv Opt Mater* 6(24):1800836
15. Zhang H, Tang D, Knize RJ, Zhao L, Bao Q, Loh KP (2010) Graphene mode locked, wavelength-tunable, dissipative soliton fiber laser. *Appl Phys Lett* 96(11):111112
16. Zhang H, Tang D, Zhao L, Bao Q, Loh K (2009) Large energy mode locking of an erbium-doped fiber laser with atomic layer graphene. *Opt Express* 17(20):17630–17635
17. Bao Q, Zhang H, Wang Y, Ni Z, Yan Y, Shen ZX, Loh KP, Tang DY (2009) Atomic-layer graphene as a saturable absorber for ultrafast pulsed lasers. *Adv Func Mater* 19(19):3077–3083
18. Cunning B, Brown C, Kielpinski D (2011) Low-loss flake-graphene saturable absorber mirror for laser mode-locking at sub-200-fs pulse duration. *Appl Phys Lett* 99(26):261109

Publisher's Note Springer Nature remains neutral with regard to jurisdictional claims in published maps and institutional affiliations.